Available online at www.sciencedirect.com
SCIENCE DIRECT®
PERGAMON
Vacuum 69 (2003) 37–52
VACUUM
SURFACE ENGINEERING, SURFACE INSTRUMENTATION & VACUUM TECHNOLOGY
www.elsevier.com/locate/vacuum

Numerical modelling of gas discharge plasmas for various applications

Annemie Bogaerts, Renaat Gijbels*

Department of Chemistry, University of Antwerp (UIA), Universiteitsplein 1, B-2610 Wilrijk-Antwerp, Belgium

Received 15 March 2002; received in revised form 1 April 2002

Abstract

Gas discharge plasmas are used for a wide range of applications. To improve our understanding about gas discharges, which is necessary to obtain good results in the various application fields, we perform numerical modelling of gas discharge plasmas. Various kinds of modelling approaches, for various types of gas discharges, are being used in our group. In this paper, some examples of this modelling work are outlined.

Keywords: Gas discharge; Plasma; Numerical modelling

1. Introduction

Gas discharge plasmas are used in many growing application fields, such as in the semiconductor industry (deposition, etching, surface modification, in different steps of integrated circuit manufacturing) [1–3], in materials technology (e.g., for the deposition of hard, protective coatings or for plasma polymerization) [4–8], in analytical chemistry (for the trace and ultra-trace analysis of (mainly) solid materials) [9,10], as light sources [11–13], gas lasers [14–16], in flat plasma display panels [17,18], as well as for environmental [19–21] and biomedical applications [22–23]. To make progress in these application fields, a good insight into the plasma processes is desirable. We try to obtain this by numerical modelling.

Different kinds of modelling approach have been applied in the literature to describe gas discharge plasmas, i.e., analytical models, fluid models, collisional-radiative (CR) models, non-equilibrium Boltzmann equations, Monte Carlo (MC) simulations, particle-in-cell (PIC) models, or a combination of these models, i.e., so-called hybrid models. Each of these models has its particular advantages and disadvantages. An *analytical model* [24,25] is very fast and can easily predict the plasma behaviour, but it is only an approximation, valid for a limited range of conditions. A *fluid model* [26,27] is based on the first velocity moments of the Boltzmann transport equation (continuity equations of particle density, momentum density and energy density), usually coupled to Poisson's equation to obtain a self-consistent electric field distribution. It is in principle also quite simple and fast (although it can be tricky to solve the set of coupled differential equations), but it is also approximate. Indeed, it

*Corresponding author. Tel.: +32-3820-2360; fax: +32-3-820-2376.
E-mail address: gijbels@uia.ua.ac.be (R. Gijbels).

0042-207X/03/$ - see front matter
PII: S0042-207X(02)00306-8

assumes more or less equilibrium with the electric field, which is not always true, e.g., for the fast electrons in regions characterized by a strong electric field, because they gain more energy from the electric field than they lose by collisions. It should be mentioned that a special form of a fluid model, i.e. a so-called *CR model* [28,29], is typically applied to atoms and ions in excited levels. For each of these excited levels, a balance equation (particle density continuity equation) is constructed, taking into account a large number of collisional and radiative populating and depopulating processes (hence the name of this model). The non-equilibrium behaviour of the plasma species, which is not always correctly treated in a fluid approach, is fully accounted for by solving the *full Boltzmann transport equation* [30,31]. However, this approach can become mathematically very complicated, especially if more than one dimension needs to be simulated. On the other hand, *MC simulations* [32,33] are mathematically simple, and they also account correctly for the non-equilibrium behaviour, but they require a long calculation time, especially for slow-moving particles. Indeed, they treat the species as separate particles on the lowest microscopic level and in a statistical way (i.e., based on random numbers). Since a large number of particles has to be followed for sufficient statistics, this can indeed lead to long calculation times. Moreover, the MC model on its own requires a certain electric field distribution as input value, and is therefore "not self-consistent". This problem is overcome by the *PIC/MC method* [34,35], which couples MC simulations for the behaviour of ions and electrons, to the Poisson equation for a self-consistent electric field. However, this modelling approach is also very time consuming. Finally, *hybrid models* [36–39] are a combination of some of the models above (e.g., MC models for fast plasma species and fluid models for slow plasma species), in order to get rid of some of the disadvantages and to benefit from the advantages of the different models.

We use many of these modelling approaches for the various gas discharge plasmas and applications under study. In this paper, an overview will be given of the various modelling activities currently in progress, and results will be presented for some specific examples.

2. Gas discharge modelling activities performed in our group

As mentioned above, gas discharge plasmas are used in a wide range of applications. It is clear that the different applications typically require different gas discharge operating conditions, such as the way of electrical coupling (direct current (DC), alternating current (AC), capacitively coupled (CC) radio-frequency (RF), inductively coupled plasma (ICP), microwave plasma, magnetron discharge, etc.), the values of electrical power, current and voltage, the gas mixture, gas pressure and the cell dimensions. Depending on these operating conditions, some specific modelling approaches appear to be more suitable than the others. Table 1 gives an overview of the modelling approaches used in our group, as well as the applications of the gas discharge plasmas under investigation.

We started the first activities in 1993 with the modelling of analytical glow discharges (see item (1) in Table 1) and hence most results up to now have been achieved in this field. However, a few years ago, our interest was widened to other, technological, applications of gas discharge plasmas (see the other items of Table 1). For some of these activities, first results have been obtained already, and can be presented here (i.e., items 2–4). For the other activities (items 5–8), only a start has been made. Hence, it is too early to report about results, but the modelling approaches that we are trying to use, will be briefly outlined in the last section.

3. Hybrid modelling network for analytical argon glow discharges with copper cathodes

Glow discharges used for analytical applications typically operate in cylindrically symmetrical cells with a volume in the order of 1 cm^3, filled with argon at a pressure of about 0.5–5 Torr. The material to be analysed is used as the cathode of

Table 1
Overview of the modelling approaches used in our research group, for the typical applications currently of interest

Modelling approach	Application
1. Hybrid modelling network (MC—fluid—CR models)	DC, RF or pulsed glow discharges in argon, with copper cathode, used in analytical chemistry
2. Hybrid MC—fluid model	DC hollow cathode discharge (HCD), e.g., in argon/copper, used for spectroscopy or laser applications
3. Fluid model	CC RF discharge in CH_4/H_2, for plasma enhanced chemical vapour deposition (PE-CVD) of diamond-like carbon (DLC) films.
4. PIC/MC model	CC RF discharge in SiH_4/H_2, e.g., for deposition applications
5. Hybrid MC—fluid model	DC magnetron discharge in argon with copper cathode, used for sputter-deposition
6. Fluid model	AC atmospheric pressure glow discharge in helium, to be used for plasma polymerization or biomedical applications
7. PIC/MC model	CC RF discharge in $Ar/CF_4/N_2$, for etching applications in the semiconductor industry
8. Computational fluid dynamics + Hybrid MC—fluid model	Calculation of gas flow (by convection) in gas discharges (e.g., fast-flow glow discharge in analytical chemistry, or large reactors for PE-CVD of DLC films)

the glow discharge, which is sputter-bombarded by energetic plasma species. The other cell walls form the anode of the glow discharge. A typical voltage of the order of 1 kV is applied between both electrodes, which results, depending on the gas pressure, in an electrical current between 1 and 100 mA. The analytical glow discharge is typically operated in DC, CC RF or pulsed mode. Because of the rather small dimensions (e.g., distance between cathode and anode is in the order of 1 cm), it consists roughly of two regions, i.e., the *cathode dark space (CDS) or sheath* in front of the cathode (or RF-powered electrode), which is characterized by a strong electric field, and the *negative glow (NG) or plasma bulk*, which fills most of the discharge and is nearly field free.

The species assumed to be present in the plasma, include electrons, argon gas atoms, argon ions (Ar^+, Ar^{2+}, Ar_2^+), fast argon atoms, argon atoms in various excited levels, sputtered copper atoms and the corresponding copper ions, both in the ground state and in various excited levels. As indicated in Table 1, these species are described with a combination of MC, fluid and CR models, in a so-called *hybrid modelling network*.

The electrons are split up in two groups: the fast electrons, with energies large enough to cause inelastic collisions, and the slow electrons. The fast electrons, which are not in equilibrium with the electric field, are treated with a *MC model* [40]. Their trajectories are calculated using Newton's laws, whereas the collisions (i.e., occurrence of a collision, kind of collision, and new energy and direction after the collision) are treated with random numbers, in combination with scattering formulas. This procedure is repeated during successive time-steps to reach steady state, until the electrons collide at the cell walls, where they can be reflected, absorbed or cause secondary electron emission, or until they arrive in the NG and reach energies below the threshold for inelastic collisions. Indeed, the latter electrons are not important anymore as fast electrons, because they do not give rise to inelastic collisions. Their only role is to carry electrical current and to provide negative space charge, which can as well, and much more efficiently, be described in a fluid approach.

The slow electrons, together with the various argon ions (see above) are described with a fluid model [41], which consists of continuity equations and transport equations (based on diffusion and on migration in the electric field) for the slow electrons and the different ions. Moreover, these equations are coupled to Poisson's equation for a self-consistent electric field distribution. This

means that the electric field is calculated with Poisson's equation based on the densities of the charged plasma species, and is used in turn to determine the transport of these charged plasma species (by migration in the fluid model, and with the Newton's laws in the MC code). Due to the strong coupling and the severe non-linearity of the differential equations, solving this fluid model is a difficult numerical task. The method we used is based on the Scharfetter–Gummel exponential scheme [42] for the transport equations, which assumes that the particle fluxes are constant between mesh points instead of the densities. The advantage of this scheme is its ability to switch between situations where either the migration component or the diffusion component of the particle flux is dominant (i.e., strong and weak electric field, CDS and NG, respectively).

Because the *argon ions* are not really in hydrodynamic equilibrium with the strong electric field *in the CDS*, they are also described in this region with a *MC code*, as well as the *fast argon atoms*, which are created in this region from energy transfer in elastic collisions of the argon ions with argon gas atoms [43]. The principle of this MC model is the same as for the fast electrons, and will therefore not be repeated here.

The *argon atoms in excited levels* are treated with a *CR model* [44]. Sixty-four argon atomic excited levels are considered; some of them are individual levels (such as the 4s levels), but most of them are effective levels, i.e. a group of individual levels with similar excitation energy and quantum numbers. The behaviour of these levels is described with 64 coupled balance equations, taking into account a large number of populating and depopulating collisional and radiative processes, such as electron, argon ion and atom impact ionization from all levels, excitation and de-excitation between all levels, and electron–ion three-body and radiative recombination to all levels, as well as radiative decay between the levels. Moreover, some additional processes are incorporated for the 4s levels, because they play an important role in the analytical glow discharge (e.g., for Penning ionization), i.e., collisions between two 4s atoms, Penning ionization of sputtered copper atoms, two- and three-body collisions with argon ground state atoms, as well as radiation trapping (i.e., a large fraction of the emitted radiation from the 4s non-metastable levels to the ground state is re-absorbed by the ground state atoms). As the boundary condition for this model, it is assumed that all excited levels are de-excited toward the ground state at the walls.

The sputtering at the cathode is calculated with an empirical formula for the sputter yield as a function of bombarding energy [45], multiplied with the flux energy distributions of the bombarding plasma species playing a role in the sputter process (i.e., argon ions, fast argon atoms and copper ions). It is assumed that all sputtered species are in atomic form.

When the copper atoms are sputtered from the cathode, they have energies in the order of 5–10 eV. However, they lose this energy almost immediately in the first mm from the cathode, by collisions with argon gas atoms, until they are thermalized. This thermalization process of the sputtered copper atoms is simulated with a MC model [46].

The further behaviour of the thermalized sputtered copper atoms (i.e., transport, ionization and excitation), and the behaviour of the excited copper atoms and of the copper ions (in the ground state and in excited levels) is described with a CR model [47]. Eight copper atom levels, seven Cu^+ ion levels and the Cu^{2+} ions are considered. Some of the copper atom and ion levels are treated separately, whereas most of them are again grouped into effective levels. Their behaviour is again described with a set of coupled balance equations with various production and loss terms, i.e., electron and atom impact ionization from all levels, excitation and de-excitation between all levels, radiative decay between all levels, electron–ion three-body recombination to the upper copper atom and ion levels, Penning ionization by argon 4s metastable levels, and asymmetric charge transfer between copper atoms and argon ions. As the boundary condition, it is assumed that 50% of the Cu ground state atoms remain on the walls, whereas the Cu excited levels are de-excited and the Cu^+ ions are neutralized at the walls.

In analogy to the argon ions, the copper ions are not in equilibrium with the electric field in the CDS

either, and they are also treated in this region with a MC code [48], which is similar to the argon ion MC model.

Finally, it should be mentioned that, although the argon gas atoms are usually assumed to be at rest and uniformly distributed throughout the discharge, we have also developed a model to describe *argon gas heating* in dc glow discharges. The gas temperature was calculated with a *heat conduction equation*, for which the power input into the argon gas was calculated in the argon and copper ion and atom MC models, based on collisions and subsequent energy transfer to the argon gas atoms [49]. With this model a non-uniform gas temperature and hence a somewhat non-uniform argon gas density was calculated.

All these models are coupled to each other due to the interaction processes between the different plasma species, i.e., the output of one model is used as input in the other models. The models are therefore solved iteratively until final convergence is reached, which takes typically several hours up to a few days on fast professional workstations. More information about these models, as well as about the coupling of the models, can be found in the references cited above, as well as in [50–52].

This modelling network has been developed in two dimensions. Indeed, due to the cylindrical symmetry of the discharge cells under investigations, the three dimensions could be reduced to two dimensions (axial and radial direction). The models are applied to DC, CC RF and micro-second pulsed glow discharges, for various cell geometries and in a wide range of operating conditions. The typical results that have been obtained with the models, include:

- the electrical characteristics (current–voltage–pressure relations);
- the potential and electric field distributions;
- the density profiles, fluxes and energies of the various plasma species;
- information about collision processes in the plasma: collisions of the electrons, ions and atoms, the various populating and depopulating processes for the atoms and ions in excited levels;
- information about sputtering at the cathode: sputtering (erosion) rates, crater profiles due to sputtering, amount of redeposition of sputtered material;
- optical emission intensities, due to radiative decay from the excited levels; and
- prediction of variations in relative sensitivity factors for glow discharge mass spectrometry.

A few examples of typical calculation results will be illustrated here. Fig. 1 shows the calculated potential distribution (a), argon ion density profile (b), sputtered copper atom density (c) and copper ion density profile (d), at 1000 V, 0.5 Torr and ca. 3 mA, in a typical commercial cell used for glow discharge mass spectrometry (the so-called VG9000 mass spectrometer, VG Elemental). The cathode is found at the left end of the figure (at $z = 0$ cm), whereas the other cell walls are grounded (at anode potential). The small rectangles (or better: "cross-sectional rings") between $z = 0.05$ and 0.15 cm symbolize the so-called front plate ring, which is also at anode potential. Finally, the small cross-sectional ring between $z = 0$ and 0.05 cm is the insulating ring between cathode and anode.

As can be seen in Fig. 1a, the potential is equal to –1000 V at the cathode, and increases very rapidly towards zero at about 0.2 cm from the cathode. This position where the potential crosses the zero-line is defined in our model as the interface between CDS and NG. In the NG, the potential is slightly positive (about 9.5 V at the discharge conditions and cell geometry under study), and is called the "plasma potential". Finally, the potential drops again to zero at the anode walls, which are grounded.

The Ar^+ ion density, calculated for the same conditions, is presented in Fig. 1b. It is low and rather constant in the CDS, but it increases rapidly in the NG and reaches a maximum about halfway the discharge. It decreases again to low values at the anode walls. The electron density is characterized by nearly the same profile, except that it is zero in the CDS. This gives rise to a positive space charge in the CDS and nearly charge neutrality in the NG; hence, resulting in the typical potential distribution shown in Fig. 1a.

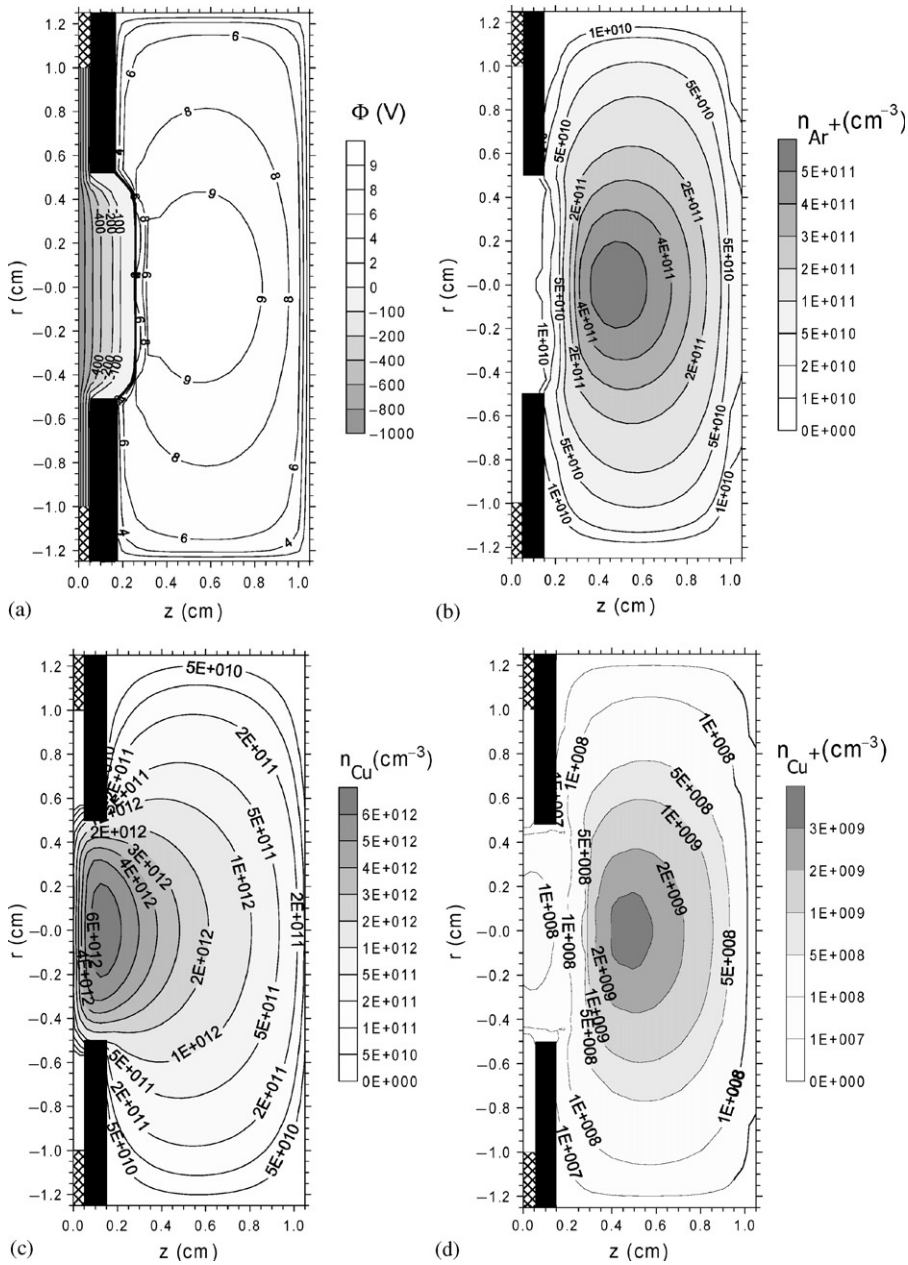

Fig. 1. Two-dimensional potential distribution (a), Ar^+ ion density (b), sputtered copper atom density (c) and Cu^+ ion density (d), in a typical glow discharge cell used for analytical mass spectrometry, at 1000 V, 0.5 Torr and 3 mA, calculated with the hybrid modelling network.

The calculated sputtered copper atom density is illustrated in Fig. 1c. It has low values at the cathode, but reaches a maximum at a few mm from the cathode and decreases gradually further in the discharge towards low values at the cell walls. In order to check this calculation result, we have performed laser-induced fluorescence measurements, albeit in a different cell geometry, for

somewhat different conditions and for tantalum instead of copper (because of availability of laser lines). The measured tantalum atom density profiles were in excellent agreement with the calculated values, both qualitatively and quantitatively, for exactly the same conditions and cell geometry [53], which suggests that the present copper atom density will also have a realistic profile.

The calculated corresponding Cu^+ ion density has a very similar profile as the Ar^+ ion density, as appears from Fig. 1d, with low and rather constant values in the CDS, and a maximum in the middle of the discharge. The absolute value is, however, two orders of magnitude lower than the argon ion density. However, if one takes into account that the copper atom density is about four orders of magnitude lower than the argon gas atom density (which is at the present conditions in the order of $10^{16}\,cm^{-3}$), this means that the copper atoms are more efficiently ionized than the argon atoms. Indeed, for argon, electron impact ionization is the dominant ionization mechanism, whereas for copper, beside electron impact ionization, also Penning ionization (by argon metastable atoms) and asymmetric charge transfer with argon ions play a role, and appear to be even more important than electron impact ionization. It is interesting to note that we have also applied laser-induced fluorescence to measure the tantalum ion density [53] and the shape of calculated and measured profiles were in excellent agreement. The calculated absolute value was, however, almost a factor of 10 too low, which is probably due to the combination of too low rate coefficients (especially for asymmetric charge transfer, which are actually unknown) in the model, as well as experimental errors (the measurements were far from straightforward). Hence, it is possible that the calculated copper ion density is also somewhat too low. This is, however, not certain, because somewhat different rate coefficients have of course been used for copper and for tantalum, and for asymmetric charge transfer of copper we found at least an estimated value in the literature, which was not the case for tantalum.

A calculation result of direct importance for analytical glow discharge spectrometry, is the crater profile at the cathode, as a result of sputtering. Indeed, the flux energy distributions of the species bombarding the cathode (argon ions, fast argon atoms and copper ions) are calculated as a function of radial position. Multiplying these flux energy distributions with a formula for the sputtering yield as a function of bombarding energy and type of bombarding particle, the flux of sputtered atoms, as a function of radial position, can be computed. From this, the crater profile at the cathode, after a certain time of sputtering, can be obtained [54]. A typical calculated crater profile, for the same conditions and cell geometry as in Fig. 1, is illustrated in Fig. 2a.

It is worth mentioning that glow discharges used in analytical spectrometry are often used to perform depth profiling, i.e., measuring the concentration in the cathode sample as a function of depth. For this purpose, flat crater profiles are desirable; if not, sample atoms originating from different depths enter the plasma simultaneously

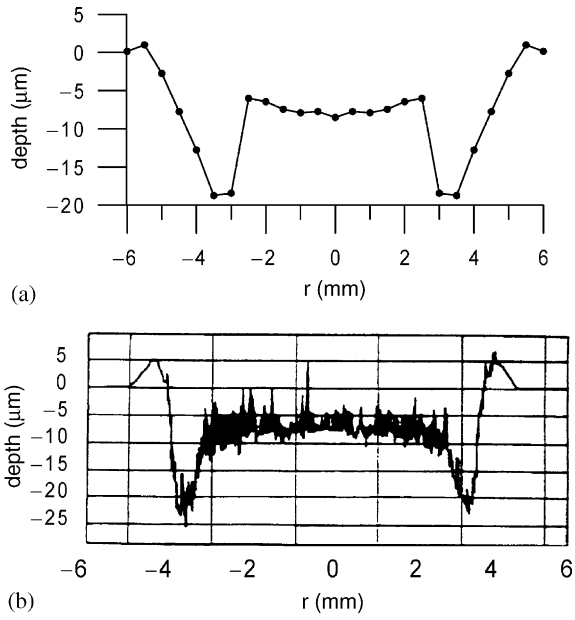

Fig. 2. Crater profiles after 45 min of sputtering on a copper cathode, in the same analytical glow discharge cell used for mass spectrometry as in Fig. 1: (a) calculated at 1000 V, 0.5 Torr and 3 mA with the hybrid modelling network, and (b) measured at 1000 V and 3 mA (pressure unknown). Reproduced from Ref. [51] with permission of the Royal Society of Chemistry.

and the depth resolution of the analysis is reduced. The crater profile presented in Fig. 2a is therefore not ideal for depth profiling. Indeed, it is much deeper at the sides than in the centre, the crater walls are not steep and the crater bottom is not flat either. Moreover, there is a small rim outside the crater profile, as a result of redeposition of sputtered material. This calculated result is, however, typical for the experimental crater profiles often encountered in glow discharge depth profiling, at least with this commercial glow discharge mass spectrometer [55]. Indeed, Fig. 2b illustrates a typical measured crater profile, obtained in the same glow discharge cell, at similar discharge conditions [55]. The measured crater profile is also much deeper at the sides than in the centre, the crater walls are not very steep (although not so pronounced as in the calculated result) and there is also a rim outside the crater profile. Hence, the calculated and experimental crater profiles are in reasonable qualitative agreement. Moreover, looking at the absolute values in the *Y*-axis tells us that the results are also in satisfactory quantitative agreement.

This example shows that the model is able to make predictions about crater profiles to be expected for a specific cell geometry and certain discharge conditions. By applying some modifications to this geometry (in particular with respect to the anode front plate; cf. Fig. 1) and/or the discharge conditions, the crater profile can, in principle, be optimized. In practice, this optimization procedure is often performed by trial and error. This can be expensive and time consuming, and leads often to disappointing results. However, the optimization can now in principle also be simulated with the model, prior to building the new cell, and this method is much cheaper and more efficient.

Finally, from the CR models which describe the behaviour of various excited levels of argon atoms, copper atoms and copper ions, we were able to calculate optical emission intensities in the glow discharge, by multiplying the level populations with the Einstein transition probabilities for radiative decay.

We have calculated optical emission spectra, based on 605 ArI lines and 103 CuI and CuII lines. The results were in reasonable agreement with spectra found in the literature [56]. Some specific ArI, CuI and CuII lines were also studied in more detail, as a function of discharge voltage and pressure, and the agreement between calculated and measured results was fairly good [57]. Moreover, in order to study the relative importance of various excitation mechanisms, we have also compared calculated spectral line intensities, as a function of distance from the cathode, with measurements at exactly the same discharge conditions and cell geometry [58].

Fig. 3a shows the calculated spatial distributions of two ArI lines, an ArII and a CuI line, at 0.6 Torr and five different currents and voltages. The corresponding experimental results [59] are plotted in Fig. 3b. It appears that the ArI 750.3 nm line, which originates from a high 4p level, shows a maximum in the beginning of the NG, due to electron impact excitation, as well as a minor peak near the cathode (in the so-called cathode glow, CG), attributed to fast argon ion and atom impact excitation. For the ArI 811.5 nm line, which originates from a low 4p level, the peak in the CG is higher than the peak in the NG. This tells us that high 4p levels are predominantly populated by electron impact excitation, which is generally accepted in the literature, but that for the low 4p levels, the most important production process at the conditions under study, is ion and atom impact excitation. The latter result is not so well known in the literature, but it follows convincingly from the good agreement between the calculated and measured emission intensities as a function of distance from the cathode.

The ArII lines are characterized by a peak in the NG, due to electron impact excitation. Indeed, for the argon ion excited levels, ion and atom impact excitation are not so important, because the ion and atom energy which would be necessary to excite the ionic levels, are much higher than the ion and atom energies typical for the glow discharge conditions under study. Finally, also the CuI lines are mainly characterized by a peak in the NG. This peak is rather broad for the CuI 324.7 nm line, as appears from Fig. 3. The reason is that this line is a resonant line (i.e., radiatively decaying to the ground state), which is subject

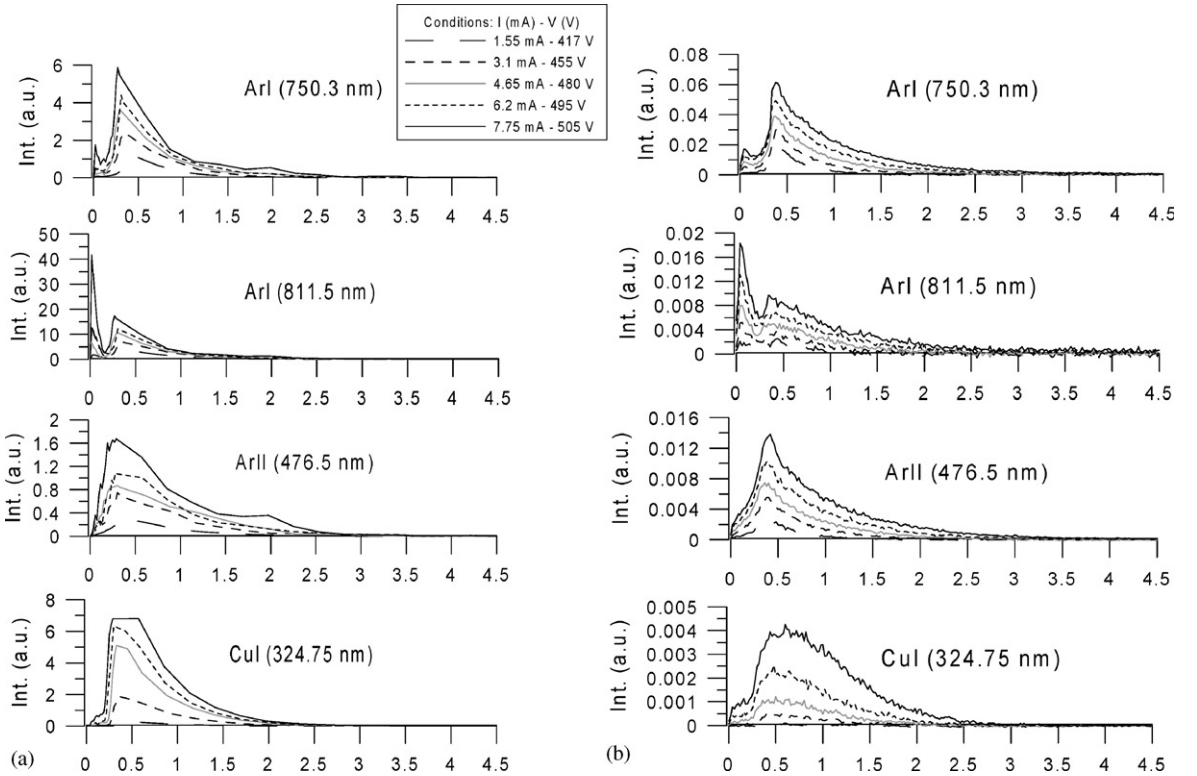

Fig. 3. Optical emission intensities as a function of distance from the cathode, in a DC argon glow discharge, at a pressure of 0.6 Torr and five different currents and voltages, for the lines: ArI (750.3 nm), ArI (811.5 nm), ArII (476.5 nm) and CuI (324.75 nm); (a) calculated with the hybrid modelling network, and (b) measured values [58].

to self-absorption [58]. In general, a good agreement has been reached between the model calculations (Fig. 3a) and the corresponding experimental data (Fig. 3b), which suggests that our model takes into account the correct excitation mechanisms and uses realistic cross-sections, and that it can therefore give more or less reliable predictions for glow-discharge optical emission spectroscopy.

In general, and as appears from the few illustrations presented above, our calculation results have been compared as much as possible with experimental data, in order to check the validity of the model (see also e.g., [50,51]). From the reasonable agreement between calculated and experimental results, it can be concluded that this hybrid modelling network presents a realistic picture of the analytical glow discharge.

4. Hybrid MC—fluid model for hollow cathode discharges (HCDs)

The hybrid MC—fluid model for fast and slow electrons and for argon (Ar^+) ions, which was developed for the analytical glow discharge, has also recently been applied to hollow cathode discharges (HCDs). The latter type of discharge, which is typically used as light source for spectroscopy or for laser applications, operates indeed at very similar discharge conditions as the analytical glow discharge. The geometry is, however, somewhat different. Indeed, the conventional glow discharge is formed by a hollow anode (i.e., the cell walls are at anode potential) and the cathode is typically a disk at one end of the hollow anode. The HCD, on the other hand, consists as the name predicts, by a cathode in the form of a hollow

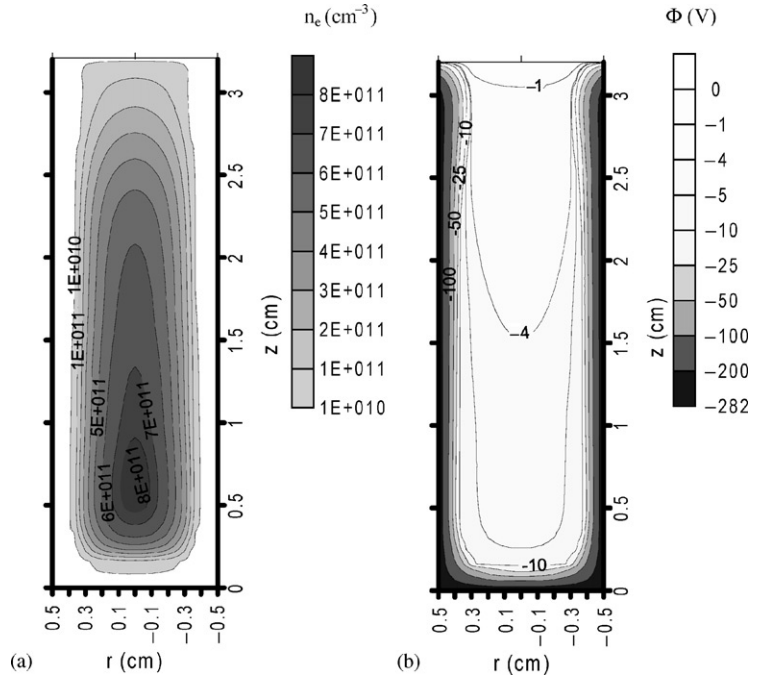

Fig. 4. Two-dimensional electron density profile (a) and potential distribution (b) in a HCD in argon with copper cathode, at 1 Torr, 282 V and 9 mA, calculated with a hybrid MC—fluid model.

tube, and the anode is a ring or disk outside the tube.

The hybrid MC—fluid model is very similar to the MC and fluid models described in Section 3; hence, we will not go into detail anymore about the model set-up. Fig. 4 shows the electron density (a) and potential distribution (b), calculated for an argon HCD with copper cathode, at 1 Torr argon gas pressure, about 300 V discharge voltage and 9 mA electrical current [60]. The cathode walls are represented by the thicker black lines at the cell borders. The anode (disk) is found at $z = 3.2$ cm. The electron density (Fig. 4a) reaches a maximum at the centre axis of the HCD, and it tends to zero at the hollow cathode walls. In the axial direction, the electron density decreases slightly towards the open end of the hollow cathode. The electrical potential (Fig. 4b) is equal to –282 V at the cathode, and it rises rapidly to about –10 V at the end of the CDS. It should be mentioned that in this model, the interface between CDS and NG is not determined by the position where the potential goes through zero, but by low values of the electric field. The NG is characterized by a small potential gradient, and by a negative plasma potential. The latter is quite striking, because glow discharges (in the common, hollow anode, geometry) are always characterized by a positive plasma potential (see also Fig. 1a). The reason is that this positive plasma potential in typical glow discharges is required to trap the electrons in the plasma. In HCDs, the electrons oscillate between opposite cathode surfaces (''pendulum effect''), and are in this way also ''trapped'' in the plasma.

5. Fluid model for a CC RF discharge in CH_4/H_2

As follows from Table 1, our modelling work is not only focused on the rare gases, but we also study gas discharges operating in reactive gases, typically used for deposition applications. One such application is the plasma-enhanced chemical vapour deposition (PE-CVD) of diamond-like

carbon (DLC) films, using a CC RF discharge in a mixture of CH_4 and H_2, for which we have recently developed a fluid model [61]. This model takes into account 20 different species, including the electrons, some neutral gases (CH_4, H_2, C_2H_6, C_2H_4, C_2H_2 and C_3H_8), ions (CH_4^+, CH_5^+, CH_3^+, $C_2H_5^+$, $C_2H_4^+$, $C_2H_2^+$, H_2^+ and H_3^+) as well as some radicals (CH_3, CH_2, CH, C_2H_5 and H).

The equations are, in analogy to the fluid model described in Section 3, the continuity (or balance) equations and the transport equations (based on diffusion and also migration for the ions and electrons) for each of the species mentioned above. Moreover, the electron energy balance equation is also added to this model, to calculate the mean electron energy (which was not necessary in Section 3, because the electron energy was there calculated in the MC model). Finally, the self-consistent electric field is again obtained from the simultaneous solution of Poisson's equation.

In total, 27 electron–neutral reactions (i.e., vibrational excitation, dissociation and ionization of the six different neutral molecules) have been included in the model, as well as 7 ion–neutral reactions and 12 neutral–neutral reactions. The ion–neutral and neutral–neutral reaction rates were calculated based on constant rate coefficients and the densities of the reacting species. To determine the electron–neutral reaction rates, on the other hand, the electron energy distribution function (EEDF) is first calculated, for a large number of electric field values, from the Boltzmann equation, using the two-term expansion. For every value of the electric field, both the average electron energy and the various reaction rate coefficients are then calculated from the EEDF, and this leads to a "look-up table", i.e., reaction rate coefficients (for every reaction) as a function of average electron energy. Hence, when the average electron energy is calculated in the fluid code from the electron energy balance equation, the electron–neutral reaction rates are consequently also defined.

Fig. 5 shows the calculated densities of the various plasma species taken into account in the model, as a function of one-dimensional distance between the two electrodes, at 0.14 Torr gas pressure, 25 W electrical power, 13.56 MHz RF frequency and 20 sccm CH_4 inlet (no H_2 inlet). It was found that besides the inlet gas (CH_4), also H_2 and the higher order hydrocarbons (C_2H_6, C_2H_4, C_2H_2 and C_3H_8) were present at relatively high densities. Moreover, the main radical was found to be CH_3, whereas the most important ions appear to be CH_5^+ and $C_2H_5^+$. The relative importance of the various plasma species has been investigated with this model, for a wide range of conditions of gas pressure, inlet fluxes, ratio of CH_4 and H_2 and electrical power.

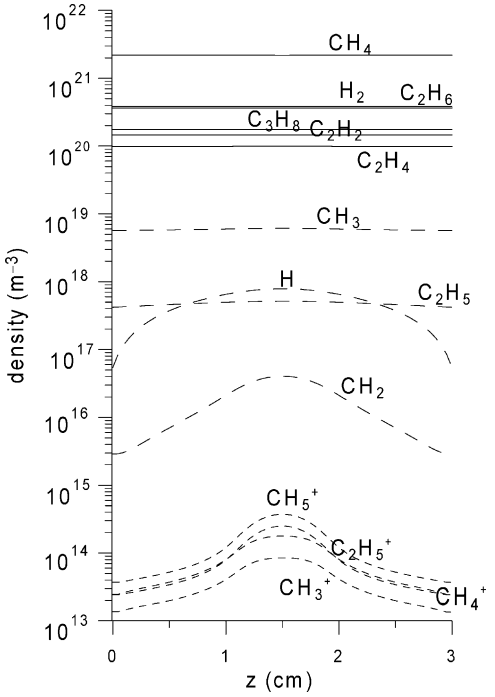

Fig. 5. Densities of the neutral molecules, the radicals, ions and electrons, as a function of distance between the electrodes, at 0.14 Torr, 25 W, 13.56 MHz and 20 sccm CH_4 inlet (no H_2 inlet), calculated with a one-dimensional fluid model for a CC RF discharge in CH_4. The neutral molecules are presented with solid lines, the radicals with long-dashed lines, and the ions with short-dashed lines. The electron density must be equal to the sum of the ion densities in the plasma, to ensure charge neutrality.

6. PIC/MC model for a CC RF SiH_4/H_2 discharge

Beside the hybrid MC—fluid model, which is described up to now to account for the non-

equilibrium behaviour of the species and to obtain self-consistent results for the electric field, the PIC/MC model, which couples a MC simulation with the solution of Poisson's equation, is also used for this purpose in our group.

The PIC/MC code was developed a few years ago by Yan and Goedheer [62,63] for a SiH_4/H_2 CC RF discharge, taking into account four different charged particles, i.e., electrons, positive ions (SiH_3^+ and H_2^+) and negative ions (SiH_3^-). Although the PIC/MC method has the advantage of being more accurate than a fluid approach, a clear disadvantage of this method is that the number of species that can be described is rather limited in comparison to a fluid model, in order not to increase the calculation time too much.

It should also be realized that the PIC/MC simulation of an electronegative gas discharge (such as in SiH_4) converges more slowly than that of an electropositive gas discharge (such as in a rare gas). This is mainly caused by the slow evolution of the negative ion density, which only depends on electron attachment and ion–ion recombination (to create and annihilate negative ions, respectively), and both these processes are characterized by very small cross-sections. Therefore, in addition to common speed-up procedures described in the literature (such as the null-collision method, different superparticle sizes and time-steps for different species; e.g., [64]), two other speed-up procedures were developed in this PIC/MC code, i.e., the so-called "rate equilibrium procedure" and the use of a low number of large-sized superparticles in the beginning of the simulation [62,63].

The above-described PIC/MC model for the electronegative SiH_4 discharge has been compared with PIC/MC results for the electropositive argon discharge, through the investigation of the electron impact ionization rate [65] and the EEDF [66] for different frequencies, pressures and power values. A significant difference between both discharge types has been found for the electric field in the plasma bulk, which is weak (several tens of V/m) in the electropositive argon discharge, and rather strong (several hundreds of V/m) in the electronegative SiH_4 discharge [66].

Recently, the PIC/MC model for the CC RF discharge in SiH_4 and in SiH_4/H_2 has also been applied to study the relaxation mechanisms after laser-induced photo-detachment, from the moment of perturbation back to equilibrium [67–69]. The latter plasma diagnostics technique is widely used in electronegative RF discharges, to measure the density, thermal energy and velocity of negative ions [70,71]. It applies photons to transform negative ions by photo-detachment into electrons and neutrals, and the subsequent increase of the electron density is detected, either by microwave cavity resonance spectroscopy, by the opto-galvanic method or by using a probe. From the measured electron density, the negative ion density can be deduced, since the loss of negative ions is equal to the production of the electrons. Moreover, from the investigation of the negative ion recovery, combined with a ballistic approximation equation, the thermal energy of the negative ions is obtained.

Since the photo-detachment method relies on the detection of the electron density, it is very important to understand the relaxation mechanism of the extra electron density and energy. The PIC/MC method is very suitable for this purpose, because it is a kinetic and a self-consistent approach. We found that laser photo-detachment has a strong influence on the discharge, which results from an increase of the electron density, leading to a weaker bulk electric field, and hence a drop in the high energy tail of the EEDF, a reduction of the reaction rates of electron impact attachment and ionization, and a subsequent decrease of the positive and negative ion densities. It was also found that the plasma quantities related to electrons recover synchronously, whereas the recovery time of the positive and negative ion densities is about 1–2 orders of magnitude longer than that of the electrons. Fig. 6 shows the one-dimensional density profiles of electrons (a), SiH_3^- ions (b) and SiH_3^+ ions (c) at various times after laser perturbation. The laser is fired at $z = 2$ cm. The solid line at "0 μs" indicates the situation immediately after photo-detachment. As expected, the electron density (Fig. 6a) shows at this moment a pronounced increase at $z = 2$ cm, whereas the SiH_3^- density drops to zero at this

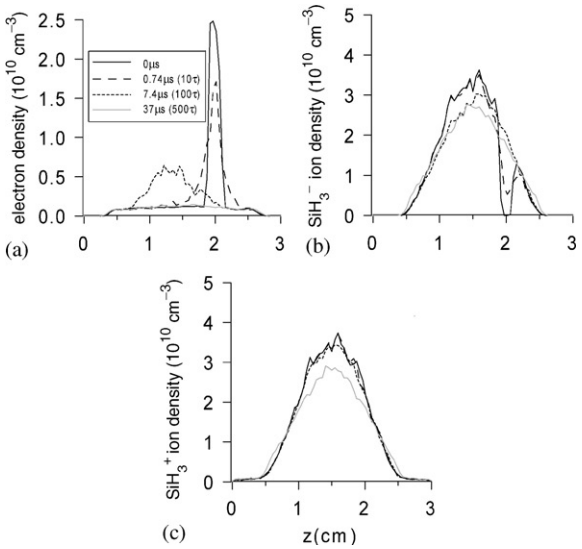

Fig. 6. Density profiles of electrons (a), SiH_3^- (b) and SiH_3^+ (c) ions, calculated with a PIC/MC model for a CC RF discharge in SiH_4, at 0.4 Torr, 13.56 MHz and 7.5 W, at various times after laser-induced photo-detachment. "0 μs" means at the time of photo-detachment. The laser impact position is at $z = 2$ cm. τ stands for the time-period of one RF-cycle.

moment (as is imposed by the assumptions in the model [68]). The SiH_3^+ density experiences no immediate effect of photo-detachment. From now on, the densities of electrons, positive and negative ions relax gradually to the initial situation. It is clear from Fig. 6a that the electron density profile has recovered almost completely after 37 μs (or 500 RF cycles), at the conditions under study (0.4 Torr, 13.56 MHz and 7.5 W electrical power). The positive and negative ion densities, on the other hand, have not yet recovered at this time, as appears from Figs. 6b and c. The typical (positive and negative) ion recovery time is in the order of 600 μs at 0.4 Torr, which is indeed more than one order of magnitude longer than the recovery time of electrons. The reason for these different recovery times is attributed to different recovery mechanisms. Indeed, the recovery time for the electrons depends on the electron diffusion speed, while for the ions, it is determined by the net increment of the production and the loss rate. Finally, it should be mentioned that the modelled behaviour of all the charged particles agrees very well with experimental results from the literature [67,68].

7. Other modelling activities currently under development in our group

7.1. Hybrid MC—fluid model for a magnetron discharge in argon

A magnetron discharge is a DC (or RF) discharge, which is not only characterized by an electric field, but to which also a magnetic field is applied. Because of this additional magnetic field, the electrons move around the magnetic field lines, increasing their travel distance in the plasma, hereby enhancing ionization. Therefore, the gas pressure in magnetron discharges is typically several orders of magnitude lower (order of a few mTorr) than in conventional glow discharges.

At this low pressure, a pure fluid code would be too rough an approximation, because the electrons do not undergo many collisions, and they can gain more energy from the electric field than they lose by collisions; hence, they are not in equilibrium with the electric field. A PIC/MC model would be a suitable approach, but it would require a very long calculation time, due to the long travel distances of the electrons. A hybrid MC—fluid model is, therefore, a good alternative, because it accounts for the non-equilibrium behaviour of the electrons with the MC method, and it reduces the calculation time with the fluid model. Introducing the magnetic field in the MC code, occurs by adding a Lorentz force term to the Newton's equations. However, introducing the magnetic field in the fluid code appears to be a much more difficult numerical task, due to fact that the magnetic field is not curl-free, which leads to coupling between the components of mass flux. In first instance, a 2D electric field and a 1D constant magnetic field, perpendicular to the electric field, are assumed. These assumptions will make it possible, after some mathematical manipulations, to uncouple the components of the mass flux, and to solve the transport equations for electrons and ions self-consistently with Poisson's equation for the electric field.

7.2. Fluid model for an AC atmospheric pressure glow discharge in helium

The atmospheric pressure glow discharge (APGD) is gaining increasing interest in recent years for many applications, such as for surface modification of polymers (to increase the wettability), plastics and fibres, for deposition of thin films, for sterilization in medical and biological applications, for ozone synthesis as well as for plasma polymerization. The advantage of the APGD is that no vacuum is required, hence reducing the operation cost and enabling on-line processing. Moreover, the APGD is more homogeneous than the (filamentary) corona and dielectric barrier discharges (DBDs), which is a prerequisite for reproducible and uniform plasma processing.

The glow discharge can only operate in the atmospheric pressure regime when at least one of both electrodes is covered with a dielectric barrier, like in a DBD. Analogously, the APGD operates in AC mode, typically in the frequency range of a few kHz.

Because of the high pressure operation, the plasma species, including the electrons, will be subject to a large number of collisions, yielding a hydrodynamic equilibrium with the electric field. Therefore, a fluid code is a suitable modelling approach for this type of discharge. A similar fluid code as described in Section 3 can be applied. However, because of the presence of a dielectric barrier, the boundary conditions at the electrodes are somewhat different and require the introduction of a ''memory voltage'', which accounts for the capacity of the dielectric barrier [72].

7.3. PIC/MC model for a CC RF discharge in a mixture of argon/CF_4/N_2

The PIC/MC model described in Section 6 is also being applied to a mixture of argon/CF_4/N_2, which is used in the semiconductor industry for etching applications. Typical operating conditions are a gas pressure of 30 mTorr, an electrical power of about 1 kW, and a gas mixture of 400 sccm Ar, 38 sccm CF_4 and 45 sccm N_2. Six different species will be taken into account in the model, including the electrons, Ar^+, CF_3^+, CF_3^-, F^- and N_2^+ ions. The collisions that will be implemented in the model are electron–argon, electron–CF_4 and electron–N_2 collisions, Ar^+–Ar collisions and CF_3^+, CF_3^- and F^- collisions with CF_4, as well as positive–negative ion and electron–positive ion recombination, and electron detachment from negative ions.

7.4. Calculation of transport by convection in gas discharge plasmas

Finally, it should be mentioned that in all the models presented above, transport is described by diffusion and also by migration for the charged particles. However, for some applications, convection will also play a role as transport mechanism. Indeed, in analytical glow discharges, a recent trend is observed to considerably increase the argon gas flow. Hence, whereas in the present models, the background gas is typically assumed to be uniformly distributed and at thermal velocities (except for the calculation of gas heating, see Section 3), this assumption will not hold true if a considerable gas flow is put into the discharge. Therefore, we are currently trying to calculate the transport by convection of the argon gas atoms in an analytical glow discharge, with a computational fluid dynamics (CFD) code. The output of this code, i.e., the density and velocity distribution of the background argon gas atoms, will be used as input in the hybrid modelling network described in Section 3. Indeed, an additional term, attributed to convection, will be added to the transport equation of ions in the fluid model.

A similar approach will also be applied in the near future to the CC RF discharge in the mixture of CH_4/H_2. Indeed, experimental research is going on to increase the size of reactors for the PE-CVD of DLC layers, in order to deposit the films on larger surfaces. Whereas in a small reactor, transport of the plasma species will predominantly be governed by diffusion and migration, this will probably not hold true for the larger reactors, where convection will also come into play. Hence, this problem will also be attacked by combining the CFD code with the plasma model for the CC RF discharge in the mixture of CH_4/H_2.

8. Conclusion

This paper intended to give an overview of possible applications of gas discharge plasmas, and the different modelling approaches that can be applied to obtain a better understanding of the plasma behaviour. As there are many different applications of gas discharge plasmas, there are as many different gas discharge operating conditions. Depending on these operating conditions, one or another modelling approach will be more suitable.

Acknowledgements

A. Bogaerts is indebted to the Flemish Fund for Scientific Research (FWO) for financial support. This research is also sponsored by the Federal Services for Scientific, Technical and Cultural Affairs of the Prime Minister's Office (DWTC/SSTC) through IUAP-IV (Conv. P4/10). Finally, the authors also greatly acknowledge the contributions to this paper from all co-workers in our group: Dr. Min Yan, Dr. A. Okhrimovskii, N. Baguer, M. Madani, V. Georgieva, I. Kolev, E. Neyts and D. Herrebout.

References

[1] Lieberman MA, Lichtenberg AJ. Principles of plasma discharges and materials processing. New York: Wiley, 1994.
[2] Grill A. Cold plasma in materials fabrication: from fundamentals to applications. New York: IEEE Press, 1994.
[3] Lieberman MA. Plasma discharges for materials processing and display applications. In: Schlüter H, Shivarova A, editors. Advanced technologies based on wave and beam generated plasmas, NATO Science Series, vol. 67. Dordrecht: Kluwer, 1999. p. 1–22.
[4] Konuma M. Film deposition by plasma techniques. New York: Springer, 1992.
[5] Bruno G, Capezutto P, Madan A, editors. Plasma deposition of amorphous silicon-based materials. San Diego: Academic Press, 1995.
[6] Wilhelm R. Deposition properties and applications of carbon-based coatings. In: Schlüter H, Shivarova A, editors. Advanced technologies based on wave and beam generated plasmas, NATO Science Series, vol. 67. Dordrecht: Kluwer, 1999. p. 123–35.
[7] Yasuda HK, editors. Plasma polymerization and plasma interactions with polymeric materials. New York: Wiley, 1990.
[8] d'Agostino R, editor. Deposition, treatment and etching of polymers. New York: Academic Press, 1990.
[9] Marcus RK. Glow discharge spectroscopies. New York: Plenum Press, 1993.
[10] Payling R, Jones D, Bengtson A. Glow discharge optical emission spectrometry. Chichester: Wiley, 1997.
[11] Abeywickrama MG. Fluorescent lamps. In: Coaton JR, Marsden AM, editors. Lamps and lighting. London: Arnold, 1997. p. 194–215.
[12] de Groot J, van Vliet J. The high-pressure sodium lamp, Philips technical library. Deventer: Kluwer, 1986.
[13] Wharmby DO. Electrodeless Lamps. In: Coaton JR, Marsden AM, editors. Lamps and lighting. London: Arnold, 1997. p. 216–26.
[14] Wilson J, Hawkes JFB. Lasers: principles and applications. New York: Prentice-Hall, 1987.
[15] Ivanov IG, Latush EL, Sem MF. Metal vapor ion lasers. Chichester: Wiley, 1996.
[16] Little CE. Metal vapor lasers. Chichester: Wiley, 1999.
[17] Weber LF. Plasma displays. In: Tannas Jr LE, editor. Flat panel displays and CRTs. New York: Van Nostrand Reinhold, 1985. p. 332–414.
[18] Sobel A. Plasma displays. IEEE Trans Plasma Sci 1991;19:1032–47.
[19] Hammer T. Applications of plasma technology in environmental techniques. Contrib Plasma Phys 1999;39:441–62.
[20] Manheimer W, Sugiyama LE, Stix TH, editors. Plasma science and the environment. Woodbury, NY: American Institute of Physics, 1997.
[21] Penetrante BM, Schultheis SE, editors. Non-thermal plasma techniques for pollution control, NATO ASI Series, Series G: Ecological Sciences, vol. 34, Part A&B. Berlin: Springer, 1993.
[22] Laroussi M. Sterilization of contaminated matter with an atmospheric pressure plasma. IEEE Trans Plasma Sci 1996;24:1188–91.
[23] Kelly Winterberg K, Hodge A, Montie TC, Deleanu L, Sherman DM, Roth JR, Tsai PP-Y, Wadsworth LC. Use of a one-atmosphere uniform glow discharge plasma to kill a broad spectrum of micro-organisms. J Vac Sci Technol 1999;17:1539–44.
[24] Berezhnoi SV, Kaganovich ID, Tsendin LD, Schweigert VA. Appl Phys Lett 1996;69:2341.
[25] Lee YT, Lieberman MA, Lichtenberg AJ, Bose F, Baltes H, Patrick R. J Vac Sci Technol A 1997;15:113.
[26] Boeuf J-P. Phys Rev A 1987;36:2782.
[27] Passchier JDP, Goedheer WJ. J Appl Phys 1993;73:1073.
[28] van der Sijde B, van der Mullen JJAM, Schram DC. Beitr Plasmaphys 1984;24:447.
[29] Vlcek J. J Phys D 1989;22:623.
[30] Abril I. Comput Phys Commun 1988;51:413.
[31] Carman RJ. J Phys D 1989;22:55.
[32] Kushner MJ. IEEE Trans Plasma Sci 1986;14:188.

[33] Donko Z, Rozsa K, Tobin RC. J Phys D 1996;29:105.
[34] Surendra M, Graves DB. IEEE Trans Plasma Sci 1991;19:144.
[35] Smith HB, Charles C, Boswell RW, Kuwahara H. J Appl Phys 1997;82:561.
[36] Surendra M, Graves DB, Jellum GM. Phys Rev A 1990;41:1112.
[37] Ventzek PLG, Hoekstra RJ, Sommerer TJ, Kushner M. J Appl Phys Lett 1993;63:605.
[38] Huang FY, Kushner MJ. J Appl Phys 1995;78:5909.
[39] Donko Z. Phys Rev E 1998;57:7126.
[40] Bogaerts A, van Straaten M, Gijbels R. Spectrochim Acta Part B 1995;50:179.
[41] Bogaerts A, Gijbels R, Goedheer WJ. J Appl Phys 1996;78:2233.
[42] Scharfetter DL, Gummel HK. IEEE Trans Electron Devices 1969;16:64.
[43] Bogaerts A, Gijbels R. J Appl Phys 1995;78:6427.
[44] Bogaerts A, Gijbels R, Vlcek J. J Appl Phys 1998; 84:121.
[45] Matsunami N, Yamamura Y, Itikawa Y, Itoh N, Kazumata Y, Miyagawa S, Morita K, Shimizu R, Tawara H. At Data Nucl Data Tables 1984;31:1–80.
[46] Bogaerts A, van Straaten M, Gijbels R. J Appl Phys 1995;77:1868.
[47] Bogaerts A, Gijbels R, Carman R. J Spectrochim Acta Part B 1998;53:1697.
[48] Bogaerts A, Gijbels R. J Appl Phys 1996;79:1279.
[49] Bogaerts A, Gijbels R, Serikov VV. J Appl Phys 2000;87:8334.
[50] Bogaerts A. Plasma Sources Sci Technol 1999;8:210–29.
[51] Bogaerts A, Gijbels R. J Anal At Spectrom 1998;13: 945–53.
[52] Bogaerts A, Gijbels R. Plasma Phys Rep 1998;24:621–32.
[53] Bogaerts A, Wagner E, Smith BW, Winefordner JD, Pollmann D, Harrison WW, Gijbels R. Spectrochim Acta Part B 1997;52:205–18.
[54] Bogaerts A, Gijbels R. Spectrochim Acta Part B 1997;52:765.
[55] Jonkers C. Ph.D. dissertation, University of Antwerp, Antwerp, 1995.
[56] Bogaerts A, Gijbels R, Vlcek J. Spectrochim Acta Part B 1998;53:1517.
[57] Bogaerts A, Wilken L, Hoffmann V, Gijbels R, Wetzig K. Spectrochim Acta Part B 2001;56:551–64.
[58] Bogaerts A, Donko Z, Kutasi K, Bano G, Pinhao N, Pinheiro M. Spectrochim Acta Part B 2000;55:1465–79.
[59] Donko Z, Bano G, Szalai L, Kutasi K, Rosza K, Pinheiro M, Pinhao N. J Phys D 1999;32:2416–25.
[60] Baguer N, Bogaerts A, Gijbels R. Spectrochim Acta Part B 2002;57:311–26.
[61] Herrebout D, Bogaerts A, Yan M, Goedheer WJ, Dekempeneer E, Gijbels R. J Appl Phys 2001;90:570–9.
[62] Yan M, Goedheer WJ. J IEEE Trans Plasma Sci 1999;27:1399.
[63] Yan M, Goedheer WJ. J Plasma Sources Sci Technol 1999;8:349.
[64] Birdsall CK. IEEE Trans Plasma Sci 1991;19:65.
[65] Yan M, Bogaerts A, Gijbels R, Goedheer WJ. J Appl Phys 2000;87:3628.
[66] Yan M, Bogaerts A, Gijbels R, Goedheer WJ. J Plasma Sources Sci Technol 2000;9:583.
[67] Yan M, Bogaerts A, Gijbels R, Goedheer WJ. J Phys Rev E 2001;63:026405.
[68] Yan M, Bogaerts A, Gijbels R, Goedheer WJ. J Phys Rev E 2002;65:16408.
[69] Yan M, Bogaerts A, Gijbels R. IEEE Trans Plasma Sci, in press.
[70] Haverlag M, Kono A, Passchier D, Kroesen HMW, Goedheer WJ. J Appl Phys 1991;70:3472.
[71] Bacal M, Berlemont PI, Bruneteau AM, Leroy R, Stern RA. J Appl Phys 1991;70:1212.
[72] Massines F, Gadri RB, Decomps P, Rabehi A, Ségur P, Mayoux C. J Appl Phys 1998;83:2950–7.